IOP Publishing Physica Scripta
Phys. Scr. 95 (2020) 044003 (7pp) https://doi.org/10.1088/1402-4896/ab5baa

Exploring the effect of aliovalent substitution of Pb^{2+} by Eu^{3+} on structural, morphological and optical properties of $CH_3NH_3PbI_3$ perovskite films

S Derbali[1,2,6], K Nouneh[1], M Florea[3], F Neatu[4], S Neatu[4], L N Leonat[3], M Secu[5], A G Tomulescu[3], V Stancu[3], L Pintilie[3], M Ebn Touhami[2] and A C Galca[3,6]

[1] Laboratory of Condensed Matter Physics, Department of Physics, Ibn Tofail University, 14000 Kenitra, Morocco
[2] Laboratory of Materials and Environment Engineering: Modeling and Application, Department of Chemistry, Ibn Tofail University, 14000 Kenitra, Morocco
[3] Laboratory of Multifunctional Materials and Structures, National Institute of Materials Physics, 077125 Magurele, Romania
[4] Laboratory of Nanoscale Condensed Matter, National Institute of Materials Physics, 077125 Magurele, Romania
[5] Laboratory of Optical Processes in Nanostructured Materials, National Institute of Materials Physics, 077125 Magurele, Romania

E-mail: sarah.derbali@uit.ac.ma and ac_galca@infim.ro

Received 9 August 2019, revised 12 November 2019
Accepted for publication 26 November 2019
Published 12 February 2020

Abstract

In this work, the effect of aliovalent substitution of Pb^{2+} by Eu^{3+} on structural, morphological and optical properties of $CH_3NH_3PbI_3$ ($MAPbI_3$) was studied, aiming to improve the properties of perovskite films used in solar cells application. The surface morphology, the microstructure and the optical properties of the obtained films containing different Europium (Eu) concentrations were characterized by atomic force microscopy, x-ray photoelectron spectroscopy, x-ray diffraction, UV–vis spectroscopy and photoluminescence spectroscopy.

Keywords: perovskite films, structural and morphological characterization, aliovalent substitution, optical properties

(Some figures may appear in colour only in the online journal)

1. Introduction

The hybrid solar cells based on organic-inorganic perovskite materials have experienced significant progress over the last decade. This can be attributed to their peculiar optical and electronic properties: a large absorption coefficient [1], possibility to tune the bandgap [2] for a good light absorption, a small exciton binding energy that allows an easy separation of charges (50 meV) [3], a large carrier mobility ($12.5\,cm^2\,V^{-1}\,s^{-1}$ for electrons and $7.5\,cm^2\,V^{-1}\,s^{-1}$ for holes) [4] and long carrier diffusion lengths (100–1000 nm) [5–7]. Additional advantages including simple solution process, low manufacturing costs, flexibility, light-weight and semi-transparency make from the organometallic perovskites ones of the most promising photovoltaic materials towards the third generation solar cells [8, 9]. To date, the power conversion efficiency (PCE) has reached over 20% for perovskite-based solar cells by [10, 11] and the research is still ongoing.

[6] Authors to whom any correspondence should be addressed.

The hybrid perovskite adopts the following chemical formula ABX_3, where A is a monovalent organic cation (mainly MA: $CH_3NH_3^+$ or FA: $HC(NH_2)_2^+$); B is divalent metal cation (mainly Pb^{2+}, Sn^{2+} or Sb^{2+}) and X is monovalent halide anion (mainly Cl^-, Br^-, or I^-) [12]. Various methods have been employed to prepare hybrid perovskite films using solution processing-based methods [13] including spin coating [14] and roll to roll printing [15]and the vapor-assisted techniques [14, 16] such as chemical vapor deposition [17] and physical vapor deposition [18]. The morphology and the structure of perovskite thin films as well as the charge carrier mobility, lifetime, are within the key parameters, which control the final performance of the perovskite solar cells [13, 19, 20]. Numerous approaches including compositional engineering and doping engineering have been experienced to find out several parameters and properties aiming to improve the structural stability and the light conversion in the perovskite films [21, 22]. It was reported that the potassium showed a positive effect on the perovskite films, by providing a good structural stability and optimum bandgap (1.5 eV) for solar cell application [23]. On the other hand, the use of the alkaline earth including barium as a doping element demonstrates an increase on the absorption and on the charge separation efficiency, reaching a champion cell with PCE of 14.9%, 3.0 mole % of Ba^{2+} was used [24]. Rare-earth (RE) elements have attracted much attention since 1966, they were used in lasers, bio-imaging, catalysis and as doping elements in the photovoltaic field [25–29]. For example, Ce^{3+}, Tb^{3+} and Yb^{3+} have been successfully introduced in perovskite films, the obtained doped films exhibit high crystalline quality with larger grain sizes, lower defect density with reduced grain boundaries compared to undoped counterparts [22, 30]. Among RE elements, europium ions (Eu^{3+}) have been widely used in different applications because of its interesting properties, but there is scarce information in literature about its behaviour in solar cells [31]. The excited f-electrons of Eu^{3+} have the ability to absorb energy from UV light by moving temporarily to a higher energy level and to return to their original state before emitting energy as visible light [32]. In dye sensitized solar cells (DSSCs), the addition of $SrAl_2O_4$:Eu^{3+} has extended the absorption range from UV light to visible light through luminescence of Eu^{3+}, thus improving the light harvesting and consequently the DSSCs photovoltaic performance [33].

In this paper, we report the results of aliovalent substitution of Pb^{2+} by Eu^{3+} in $MAPbI_3$-Eu% perovskite films. We first describe the synthesis and the deposition of pristine and doped perovskite films, using a one-step spin coating method. Then, we depict the structural, morphological and optical characterization of the prepared $MAPbI_3$-Eu% perovskite films.

2. Experimental section

2.1. Materials

Ti-Nanoxide T/SP was purchased from Solaronix, while methylammonium iodide (MAI), lead iodide (PbI_2), europium nitrate $Eu(NO_3)_3$, N,N-Dimethylformamide (DMF), dimethylsulfoxide (DMSO), diethyl ether, acetone, isopropanol and anhydrous ethanol were all purchased from Merck.

2.2. Solution preparation

The TiO_2 colloidal solution was prepared using Ti-Nanoxide T/SP and ethanol. The perovskite solutions $MAPb_{1-x}Eu_xI_3$, ($x = 0$, 0.01, 0.03 and 0.05, $x =$ mole fraction of doping in Pb-site), were prepared by mixing 1M of MAI and 1M of a mixed solution containing PbI_2 and $Eu(NO_3)_3$ with different mole fraction from 0% to 5% dissolved in DMF:DMSO. The solutions were stirred overnight and filtered using a μfilter of 0.2 μm afterwards.

2.3. Deposition step

The substrates used in this study are fused silica (amorphous quartz). Before utilization, the substrates were cleaned sequentially by deionized water, acetone and isopropanol for 5 min and after, cleaned in oxygen plasma for 10 min. For a good adhesion, a layer of mesoporous TiO_2 (m-TiO_2) was deposited by spray pyrolysis onto the glass substrates at 100 °C, followed by annealing at 500 °C for 1 h. The $MAPbI_3$-Eu% perovskite precursor solutions were spin-coated onto the SiO_2/m-TiO_2 with the speed of 2000 rpm for 25 s. After that, 100 μl of diethyl-ether as anti-solvent was dropped at 9 s. Last, the perovskite films were annealed at 120 °C for 3 min.

3. Characterization techniques

The as-prepared samples have been characterized using several techniques. Thus, the x-ray diffraction was performed using a Bruker-AXS D8 Advance diffractometer equipped with a LynxEye 1D detector and Cu-Kα (0.154 1nm) radiation source and a scintillation counter detector. The diffraction patterns were recorded over a 2θ range of 10°–45° with a 0.02° step size and using a counting time of 1 s per point. For the identification of the XRD phases present in the samples, the Powder Diffraction Files from the International Center for Diffraction Data (PDF-ICDD) were used. The optical densities were recorded using a V-VASE Woollam spectroscopic ellipsometer in conventional spectroscopy mode. The photoluminescence spectra were acquired using a FluoroMax 4P spectrophotometer. The surface morphology of the samples was inspected using an atomic force microscope (AFM) (NT-MDT Aura Ntegra Prima Station, the samples were scanned in the semi-contact mode). XPS measurements were performed using a Kratos Ultra DLD Setup spectrometer using the Kα of Al (1 486.74 eV) radiation produced by an x-ray source operating at a total power of 300 W

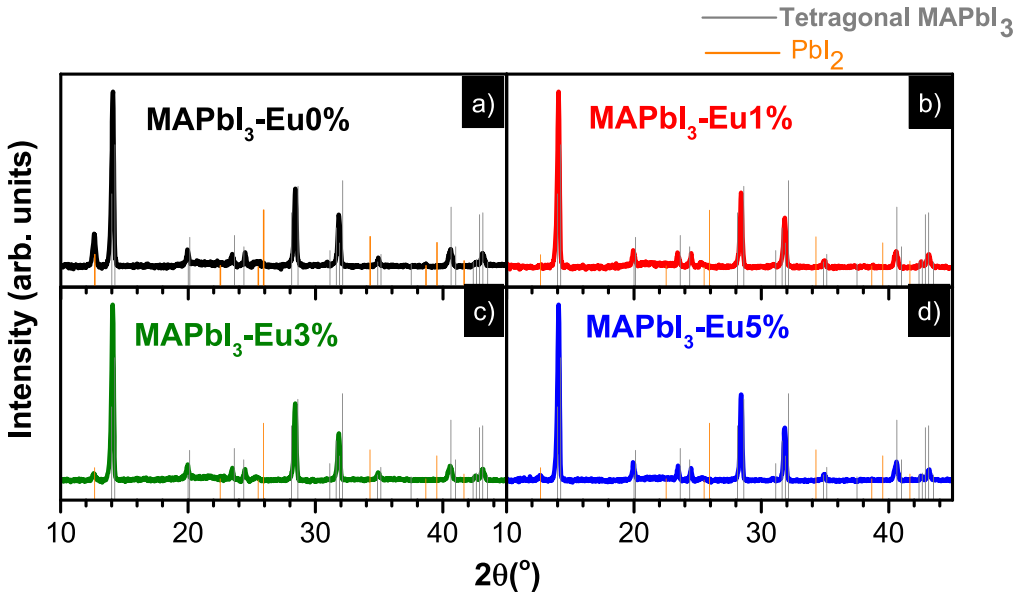

Figure 1. X-ray diffractograms of $MAPbI_3$-Eu% perovskite films.

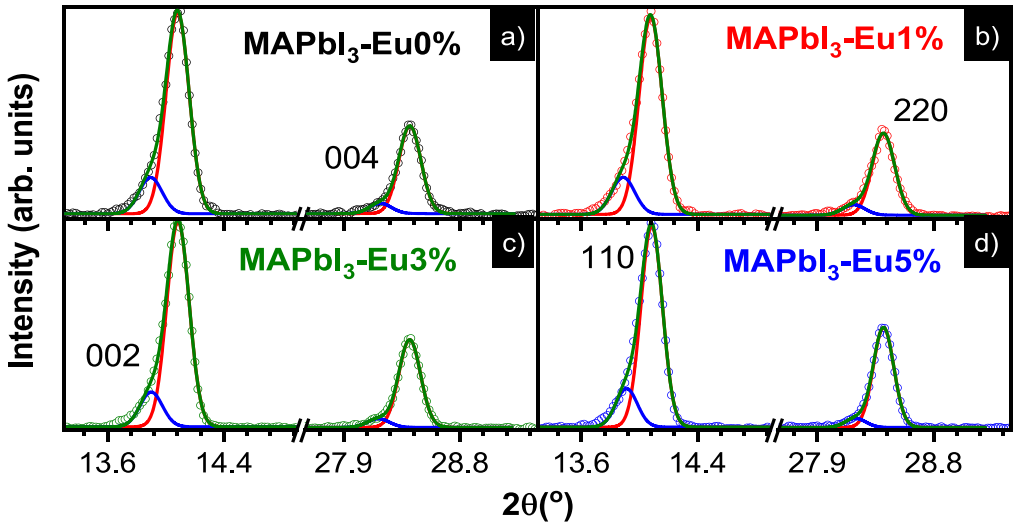

Figure 2. Selected XRD patterns of (002)/(110) and (004)/(220) reflections and the diffraction peaks of each component resulted from 2 Gaussian function fitting routine.

(12.0 kV × 25 mA) and an approx. 1×10^{-7} Pa. The spectra were calibrated using the C 1s line (BE = 284.8 eV) of the adsorbed hydrocarbon on the sample surface (C–C or $(CH)_n$ bindings).

4. Results and discussion

4.1. XRD analysis

Figure 1 shows the x-ray diffraction patterns of the films prepared using solutions containing different mole fractions of Eu: 0%, 1%, 3% and 5%, respectively. The x-ray diffraction patterns are similar for undoped and europium-doped $MAPbI_3$ films. The peaks at 14.01°, 19.99°, 23.51°, 24.48°, 28.32°, 31.93°, 35.02°, 40.62° and 42.85° correspond to the (110), (112), (211), (202), (220), (310), (312), (400), (411) planes of perovskite tetragonal crystalline structure, respectively [ICDD PDF#01 − 084 − 7607]. The partial substitution of Pb with Eu does not influences the peaks positions within the diffractometer limits, as reported previously by [34], thus the derived cell parameters a and c are merely the same ($a = 8.87$ Å and $c = 12.65$ Å). However, in figure 2 are presented the selected XRD patterns of (002)/(110) and (004)/(220) reflections and the diffraction peaks of each component resulted from 2 Gaussian function fitting routine for each pair of reflections. The broadening of the peaks becomes smaller as Eu concentration increases, suggesting that the average crystallite size is increasing upon incorporation of Europium.

On the other hand, the pristine films are marked with the secondary phase of PbI_2 characterized by 12.26° diffraction peak, while the doped films contain much less of the unreacted PbI_2, as indicated by the lowest intensity of the

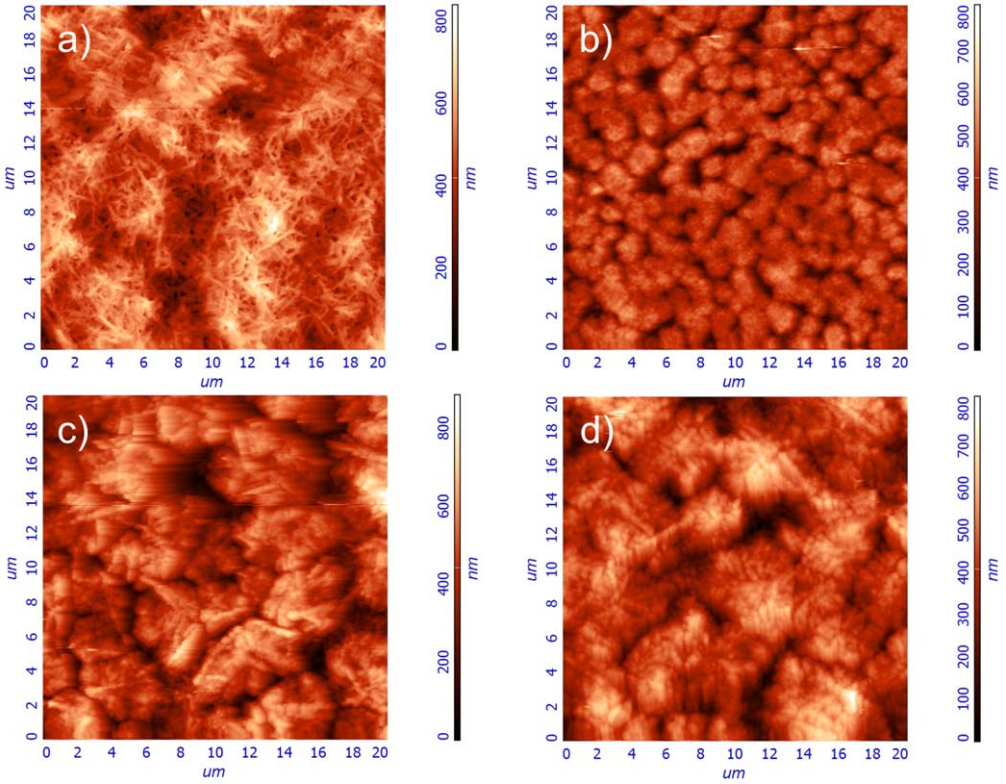

Figure 3. AFM images of $MAPbI_3$-Eu% perovskite films, (a)Eu-0%, (b) Eu-1%, (c) Eu-3%, and (d) Eu-5%.

diffraction peak characteristic to PbI_2 in samples containing Eu-3% and Eu-5%. Moreover, in the sample containing Eu-1%, the diffraction peak pertaining to PbI_2 is silent. This behaviour can be assigned to Europium incorporation, which probably increases the rate of perovskite crystallization process and thus hindering the PbI_2 formation. The same results were already reported previously, where the Eu incorporation decreases the amount of PbI_2 residue [34].

4.2. Surface morphology using AFM

The atomic force microscopy was used to explore the surface morphology of the prepared $MAPbI_3$-Eu% films (figures 3(a)–(d)). In accordance with AFM images, different morphologies were obtained for the pristine and the doped perovskite films. The pristine $MAPbI_3$ films reveal needle-like crystals that cover the substrate surface. After adding Eu, a change in the surface morphology was observed. Indeed, the AFM images reveal the formation of aggregates of grain-like structure with spaces in between. The root mean square (rms) roughness of all measured films is 96 nm, 84 nm, 119 nm, 110 nm respectively for the films with Eu-0%, Eu-1%, Eu-3% and Eu-5% in 20 × 20 μm^2 scanning area.

Compared to pristine perovskite films, the doped films with the lowest amount of Eu shown a smoother surface, which could be related to a better organization when only Eu-1% is employed. This correlates well with the x-ray diffraction of this film where the perovskite structure is without any residual PbI_2 (film with Eu1%). The formation of compact films might be beneficial for the stability of the solar device [34]. Higher concentration of Europium (Eu-3% and Eu-5%) does not lead to further improvement in the surface morphology and the rms is almost identical with slightly higher values than those of previous films (Eu-0% and Eu-1%) [35].

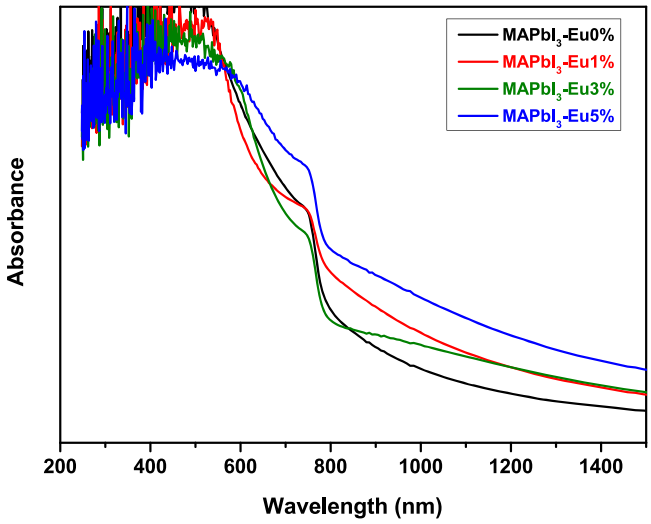

Figure 4. UV–vis absorption spectra of $MAPbI_3$-Eu% perovskite films.

4.3. UV–vis measurements

Figure 4 shows the UV–vis spectra of the as-prepared films. As can be observed, the addition of Eu leads to an increase of the absorption in the range of 700–800 nm due to the 4*f* electron transitions of Eu^{3+}. However, for the present study, the volume (thickness) of measured samples was not possible

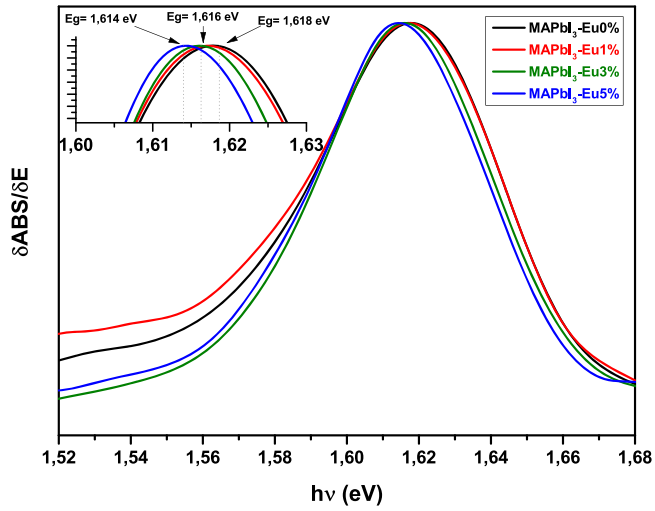

Figure 5. Derivative plots (δABS/δE) for $MAPbI_3$-Eu% perovskite films.

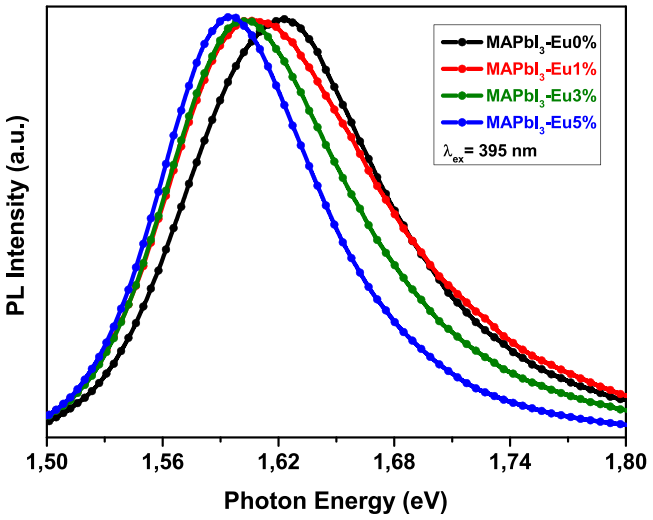

Figure 6. Photoluminescence spectra of $MAPbI_3$-Eu% perovskite films.

to be accurately measured. Due to great differences in surface morphology, the thicknesses could also differ greatly, and consequently a true comparison of absorption coefficients cannot be made.

4.4. Band gap energy

The bandgap energy can be determined easily and directly from the peak of its derivative spectrum of the absorption coefficient. The derivative spectra of the absorption for the $MAPbI_3$-Eu% films with different concentrations of Eu are depicted in figure 5. The Eg value for pristine and $MAPbI_3$-Eu% doped films is determined using the maximum values of these plots and are 1.618 eV (for Eu0% and Eu-1%), 1.616 eV (Eu-3%) and 1.614 eV (Eu-5%). The bandgap variation is relatively small. A slight shift towards the red region with Eu incorporation is observed for Eu-3% and Eu-5%. Nevertheless the obtained bandgaps matched well with the values reported in the literature and are appropriate for solar cell applications [36].

4.5. Photoluminescence properties

Figure 6 shows the normalized PL spectra for the prepared $MAPbI_3$-Eu % films. All the samples were excited by 395 nm. The emission spectra are mainly composed of one emission peak. The steady-state PL peak of $MAPbI_3$ shifts from 764 nm (1.62 eV) for pristine films to 770 nm (1.61 eV), 774 nm (1.60 eV) and 777 nm (1.59 eV) for Eu-0%, Eu-1%, Eu-3% and Eu-5% films, respectively. The maximum PL wavelength red shifted by incorporating the Europium impurity. This red shift effect might be due to a change in the band structure during the Europium incorporation into the perovskite lattice.

4.6. X-ray photoelectron spectroscopy analysis

Figure 7 displays the high-resolution spectra of Eu $3d_{5/2}$ photoelectron peaks for the films containing Eu-1%, Eu-3% and Eu-5%. The spectra are fitted well with two components with binding energies (BE) characteristic to Eu^{3+} (1 135.12 eV) and Eu^{2+} (1 125.44 eV) [37–40]. These results indicate that Eu has been successfully incorporated into the perovskite lattice, which occurs in two oxidation states of +3 and +2 and reveals different intensities for each film. In all

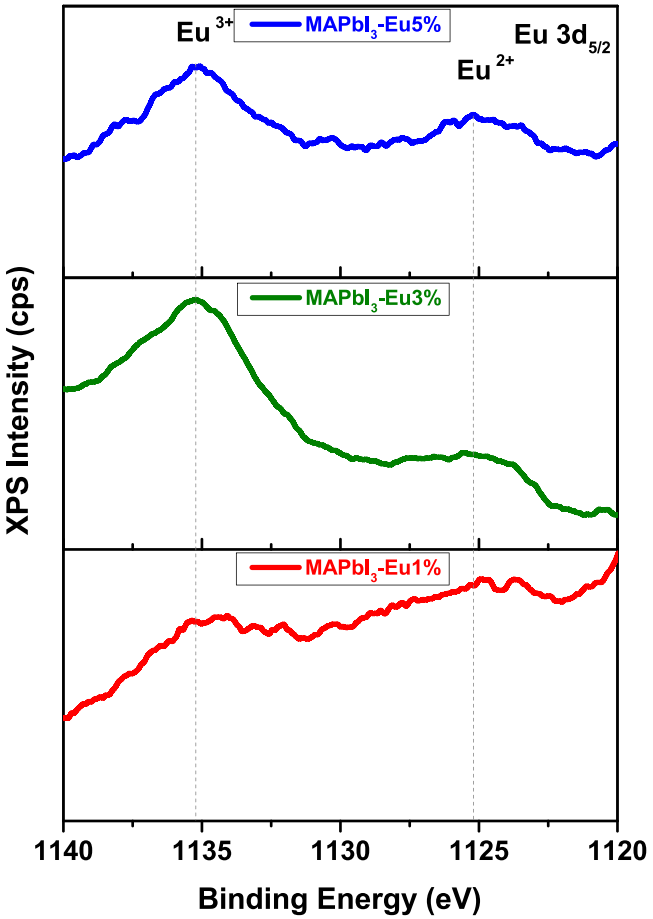

Figure 7. High-resolution spectra of Eu $3d_{5/2}$ level in the $MAPbI_3$-Eu% perovskite films.

films, the quantitative assessment indicates that the Eu^{3+} to Eu^{2+} ratio is slightly above 2.

To the best of our knowledge, the reduction of Eu^{3+} to Eu^{2+} in the air atmosphere has already been identified in several compounds with three-dimensional structures. The associated research has also suggested four conditions that appear to be important for the reduction of Eu^{3+} to Eu^{2+} when prepared in an air atmosphere. These can be summarized as follows: (1) the host compounds contain no oxidizing ions; (2) RE^{3+} (or Eu^{3+}) ion substitutes for the divalent cation in the hosts; (3) the substituted cation has a similar radius to the divalent Eu^{2+} ion; and (4) the host compound has an appropriate structure, which is composed of the tetrahedral anion groups [41–43]. In this study, the XPS results of $MAPbI_3$-Eu% doped films, reveals the coexistence of two kinds of europium (Eu^{3+} and Eu^{2+}), indicating the Eu^{3+} ions that replace Pb^{2+} are partially reduced to Eu^{2+} in the perovskite lattice. Such reduction can be described with the model of charge compensation that forces the reduction of Eu^{3+} to Eu^{2+}. The Eu^{3+} substituting for Pb^{2+} entails a change in the composition of the perovskite lattice by the formation of Pb vacancies acting as donors. Therefore, the charge compensation is ensured by lead vacancies: the negative charges of the vacancy defects would be transferred to the Eu^{3+} sites and reduce them to the divalent state.

5. Conclusion

In summary, $MAPbI_3$-Eu% perovskite films were deposited by spin coating technique. By keeping the same deposition conditions and varying only the concentrations of the salts, the aliovalent substitution of Pb^{2+} by Eu^{3+} seems to have an impact on structural, morphological and optical properties. The most important feature of this study is that the presence of Eu in low amounts (i.e. Eu-1%) hindered the formation of residual PbI_2 and promotes the formation of a dense perovskite film which can be beneficial for the device stability. However, the surface morphology study for higher Eu% concentrations indicates possible pinholes that might lead to less efficient power conversion. The doping process influences slightly the bandgap of the hybrid perovskite thin films but remains in the optimal range for solar cells applications. The aliovalent substitution of Pb^{2+} by Eu^{3+} was confirmed by XPS analysis, but the isovalent substitution cannot be excluded.

Acknowledgments

SD acknowledges Romanian Ministry of Foreign Affairs and *Agence universitaire de la Francophonie* for the *Eugen Ionescu* research and mobility grant at NIMP. All authors acknowledge the financial support from Moroccan Ministry of Higher Education and Research and CNRST in the framework of PPR/37/2015 project, and from Romanian Ministry of Research and Innovation in the framework of Core Program PN19-03 (contract no. 21 N/08.02.2019). MF, FN and SN acknowledge the Romanian National Authority for Scientific Research and Innovation, CNCS-UEFISCDI for funding through project PN-III-P4-ID-PCE-2016-0692.

ORCID iDs

S Derbali https://orcid.org/0000-0003-1663-8343
A C Galca https://orcid.org/0000-0002-1914-4210

References

[1] Ke W, Fang G, Wang J, Qin P, Tao H, Lei H, Liu Q, Dai X and Zhao X 2014 *ACS Appl. Mater. Interfaces* **6** 15959–15965
[2] Eperon G E, Stranks S D, Menelaou C, Johnston M B, Herz L M and Snaith H J 2014 *Energy Environ. Sci.* **7** 982–988
[3] Phillips L J, Rashed A M, Treharne R E, Kay J, Yates P, Mitrovic I Z, Weerakkody A, Hall S and Durose K 2016 *Sol. Energy Mater. Sol. Cells* **147** 327–333
[4] Ono L K, Raga S R, Wang S, Kato Y and Qi Y 2015 *J. Mater. Chem.* A **3** 9074–9080
[5] Zheng L, Zhang D, Ma Y, Lu Z, Chen Z, Wang S, Xiao L and Gong Q 2015 *Dalton Trans.* **44** 10582–10593
[6] Cui J, Yuan H, Li J, Xu X, Shen Y, Lin H and Wang M 2015 *Sci. Technol. Adv. Mater.* **16** 036004
[7] Chaudhary J, Choudhary S, Negi C M S, Gupta S K and Verma A S 2019 *Phys. Scr.* **94** 105821
[8] Chen L C, Tien C H, Tseng Z L and Ruan J H 2019 *Nanomaterials* **9** 121
[9] Anghel D V, Nemnes G A, Pintilie I and Manolescu A 2019 *Phys. Scr.* **94** 125809
[10] Fujiwara H, Kato M, Tamakoshi M, Miyadera T and Chikamatsu M 2018 *Phys. Status Solidi* a **215** 1700730
[11] Yang W S *et al* 2017 *Science* **356** 1376–1379
[12] Albero J, Asiri A M and García H 2016 *J. Mater. Chem.* A **4** 4353–4364
[13] Yang Y, Song J, Zhao Y, Zhu L, Gu X, Gu Y, Che M and Qiang Y 2016 *J. Alloys Compd.* **684** 84–90
[14] Kajal P, Ghosh K and Powar S 2018 Manufacturing techniques of perovskite solar cells *Appl. Solar Energy* **16** 341–364
[15] Deng Y, Peng E, Shao Y, Xiao Z, Dong Q and Huang J 2015 *Energy Environ. Sci.* **8** 1544–1550
[16] Shen P S, Chiang Y H, Li M H, Guo T F and Chen P 2016 *APL Mater.* **4** 091509
[17] Liu M, Johnston M B and Snaith H J 2013 *Nature* **501** 395–398
[18] Fan P, Gu D, Liang G X, Luo J T, Chen J L, Zheng Z H and Zhang D P 2016 *Sci Rep.* **6** 29910
[19] Kim H P, Yusoff A R B M and Jang J 2019 *Nanoscale Adv.* **1** 76–85
[20] Zhao Y, Liu J, Lu X, Gao Y, You X and Xu X 2015 *Appl. Surf. Sci.* **359** 560–566
[21] Kim H S, Hagfeldt A and Park N G 2019 *Chem. Commun.* **55** 1192–1200
[22] Zhou Y, Chen J, Bakr O M and Sun H T 2018 *Chem. Mater.* **30** 6589–6613
[23] Muzammal uz Zaman M, Imran M, Saleem A, Kamboh A H, Arshad M, Khan N A and Akhter P 2017 *Physica* B **522** 57–65
[24] Chan S H, Wu M C, Lee K M, Chen W C, Lin T H and Su W F 2017 *J. Mater. Chem.* A **5** 18044–18052
[25] Auzel F 2004 *Chem. Rev.* **104** 139–174
[26] Wang F and Liu X 2009 *Chem Soc Rev.* **38** 976–989
[27] Liang L *et al* 2013 *Adv Mater.* **25** 2174–2180

[28] Zhan W, Guo Y, Gong X, Guo Y, Wang Y and Lu G 2014 *Chin. J. Catal.* **35** 1238–1250
[29] Qiao Y, Li S, Liu W, Ran M, Lu H and Yang Y 2018 *Nanomaterials* **8** 43
[30] Rudd P N and Huang J 2019 *Trends Chem.* **1** 394–409
[31] Jena A K, Kulkarni A, Sanehira Y, Ikegami M and Miyasaka T 2018 *Chem. Mater.* **30** 6668–6674
[32] Rahman N U, Khan W U, Khan S, Chen X, Khan J, Zhao J, Yang Z, Wu M and Chi Z 2019 *J. Mater. Chem.* A **7** 6467–6474
[33] Wang L, Guo W, Hao H, Su Q, Jin S, Li H, Hu X, Qin L, Gao W and Liu G 2016 *Mater. Res. Bull.* **76** 459–465
[34] Wu X, Li H, Wang K, Sun X and Wang L 2018 *RSC Adv.* **8** 11095–111101
[35] Xiang W *et al* 2019 *Joule* **3** 205–214
[36] Yang Z, Rajagopal A and Jen A K Y 2017 *Adv. Mater.* **29** 1704418
[37] Mercier F, Alliot C, Bion L, Thromat N and Toulhoat P 2006 *J. Electron. Spectrosc. Relat. Phenom.* **150** 21–26
[38] Kumar V, Kumar V, Som S, Duvenhage M, Ntwaeaborwa O and Swart H 2014 *Appl. Surf. Sci.* **308** 419–430
[39] Lacanilao A, Wallez G, Mazerolles L, Dubot P, Binet L, Pavageau B, Servant L, Buissette V and Le Mercier T 2013 *Solid State Ion.* **253** 32–38
[40] Kang J G, Jung Y, Min B K and Sohn Y 2014 *Appl. Surf. Sci.* **314** 158–165
[41] Dai W B 2014 *J. Mater. Chem.* C **2** 3951–3959
[42] Zhang J C, Long Y Z, Zhang H D, Sun B, Han W P and Sun X Y 2014 *J. Mater. Chem.* C **2** 312–318
[43] Xie H, Lu J, Guan Y, Huang Y, Wei D and Seo H J 2014 *Inorg. Chem.* **53** 827–834